COMMUNICATION

Check for updates

Continuous hydrogenolysis of acetal-stabilized lignin in flow†

Wu Lan,‡ Yuan Peng Du, [ID] Songlan Sun, Jean Behaghel de Bueren, [ID] Florent Héroguel and Jeremy S. Luterbacher [ID] *

Using acetal-stabilized lignin we performed a truly steady state continuous high-yielding lignin depolymerization (45% monophenolics using Ni/C), which offered a window into challenges and opportunities that will be faced when processing this feedstock. With an excess of catalyst present, we observed stable depolymerization yields for 125 h time on stream. However, using catalyst loadings that were just sufficient to achieve initial maximum hydrogenolysis monomer yields revealed rapid catalyst deactivation. High yields could be partially recovered with high temperature regeneration under a reducing environment. Characterization of spent catalysts revealed that sintering and carbonaceous deposits rather than leaching were the main phenomena causing deactivation.

1. Introduction

Lignin is the most abundant aromatic polymer in nature and consists of different methoxylated phenylpropanoid units that are linked by C–C and C–O bonds.[1] It accounts for approximately 15–30% by weight and 40% by energy of lignocellulosic biomass.[2] This high energy content along with its aromaticity have led to increasing interest in lignin depolymerization for the ultimate production of sustainable fuels and aromatic chemicals in recent years.[3–7]

Hydrogenolysis, usually conducted at high temperature (180–250 °C) with a hydrogen donor (hydrogen or protic solvent) and a metal catalyst,[8–10] has led to some of the most promising results for lignin depolymerization. Under such conditions, ether bonds in the lignin polymer can be readily cleaved by what is thought to be a combination of solvolysis and surface reactions.[11] Under such conditions, unstable intermediates released from lignin are rapidly stabilized by saturation of the C=C bonds, preventing undesirable C–C condensation and therefore afford better yield of monophenolic molecules than other methods.

The aromatic monomer yield from lignin hydrogenolysis is highly dependent on the lignin structure: a higher content of ether linkages between monophenolic monomers and a lower content of C–C linkages leads to higher monomer yields. Due to the need to ether linkages on either side of a monophenolic monomer to produce a monophenolic product during depolymerization, the theoretical yield of monomers based on depolymerization by ether cleavage is thought to be roughly equal to the square of the ether linkage content in the lignin.[12,13] For native hardwoods, where ether linkages are typically around 70%, this leads to theoretical yields of monophenolic molecules around 50%.[14,15] Lignin can be very efficiently isolated under acid or base conditions but undergoes irreversible condensation, where the formation of additional C–C linkages results in low monomer yield (*e.g.* carbon yields, which are similar to the mass yields mentioned above of around 3.5–22.6%) after subsequent hydrogenolysis.[16]

To overcome these condensation limitations, several groups have developed so-called "reductive catalytic fractionation (RCF)" processes that directly depolymerizes lignin within native solid biomass without any separation process over different metal catalysts in batch conditions. Under appropriate conditions, RCF can generate aromatic monomers close to theoretical yield.[7,17–19] Though these results are promising, any eventual commercial process will likely have to be continuous to be able to produce aromatic molecules at bulk chemical prices. At the same time, RCF must still overcome catalyst separation issues due to this process requiring close contact between the metal catalyst and the biomass.

To address this issue, Román-Leshkov *et al.*[20,21] and Samec *et al.*[22] developed RCF processes in flow-through systems

where the solvent is flowed through the immobilized biomass and any reactive lignin fragments that are extracted by solvolysis are rapidly carried over a metal catalyst. At high flowrate, reactive intermediates are sufficiently rapidly brought into contact with the catalyst that close physical contact between biomass and catalyst is no longer necessary. Specifically, the catalyst and feedstock were packed in separate columns and methanol was pumped through the feedstock first to extract partially depolymerized and unstable lignin (as well as other biomass components) over a catalyst bed that performed hydrogenolysis under a hydrogen atmosphere. Both groups have shown that, with this approach, monomer yields comparable to that of batch reactors can be achieved.

However, this approach has two limitations. First, achieving rapid flowrate through biomass and to the catalyst bed that ensures limited lignin condensation requires very high solvent to solids ratios be used. Second, because the biomass bed is undergoing solvolysis as the solvent is flowed through it, the biomass is constantly evolving and the process is not steady state but transient. Complex continuous setups could be envisaged such as countercurrent screw feeders, which could ensure steady state operation but they have yet to be demonstrated. With current setups, biomass bed needs to be reloaded between runs as the lignin is consumed. This lack of truly steady state continuous operation limits possibilities that are afforded by data obtained in steady state operation, including kinetic and catalyst deactivation measurements.

Fully steady state processes have been studied using isolated lignins.[23,24] However, these lignins had either suffered from extensive condensation during the isolation process or only represented small fractions of the total lignin. Therefore, the monomer yield on the basis of the biomass's native Klason lignin content was always very low (9–14%) and thus not representative of what would be required in a realistic lignin depolymerization process. Therefore, a truly steady state continuous lignin depolymerization process that can achieve close to the maximum aromatic monomer yield has yet to be reported.

Recently, our group has developed a biomass fractionation and lignin isolation method called aldehyde assisted fractionation (AAF) that uses aldehydes to stabilize the α,γ-diol structure in lignin (Fig. 1), thus preventing the undesired condensation that would otherwise happen during lignin extraction.[25–28] This stabilized lignin can be isolated, is bench stable and can be converted to monophenolic monomers at yields that are near theoretical based on ether content and comparable to those attainable using batch-RCF processes, in a subsequent hydrogenolysis step. Here, we leveraged this method to demonstrate and characterize a fully continuous steady state lignin depolymerization process. We demonstrated that maximal yields and selectivity to aromatic monomers could be achieved but that catalysts deactivated, which gave us unique insights into the phenomena that govern continuous lignin processing. The development of such a reaction system is important in the context of developing more scalable lignin processes but also of studying reaction kinetics and catalyst stability, thus contributing to catalyst development.
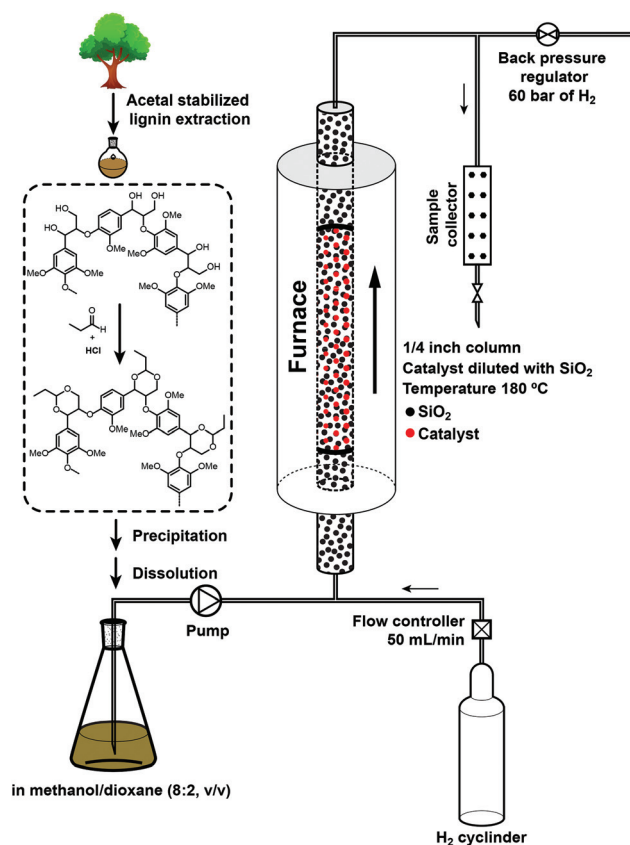

Fig. 1 Procedure and setup for the hydrogenolysis of propylene acetal stabilized lignin in a continuous flow reactor.

2. Results and discussion

We isolated propylidene acetal-stabilized lignin by pretreatment of birch particles in dioxane with hydrochloride acid and propionaldehyde at 85 °C. The resulting liquor containing stabilized lignin and carbohydrates (mainly xylose) was added to hexane to precipitate lignin while keeping propionaldehyde-functionalized xylose in solution. The resulting precipitate was collected by filtration and then washed with diethyl ether to eliminate residual carbohydrates. This isolated lignin could produce a monophenolic monomer yield of 45% (on the basis of the Klason lignin content of the original biomass, see section 4 of ESI†) after subsequent hydrogenolysis in a batch reaction with Ni/C at 200 °C for 15 h. As previously reported, this yield was close to that obtained by hydrogenolysis of the extracted liquor (47%), as well as the RCF of the original biomass (50%), suggesting that the prepared lignin sample was largely representative of native lignin.

Methanol is an efficient solvent for lignin hydrogenolysis but did not completely dissolve stabilized-lignin at room temperature, whereas dioxane can efficiently dissolved our lignin. Therefore, to prepare a feedstock solution for continuous hydrogenolysis, we re-dissolved the lignin powder in a dioxane/methanol (2 : 8, v/v) solution at a concentration of 2.5 mg mL^{-1} and filtered off any possible precipitates to avoid

clogging issues during continuously operation. Removal of the precipitates did not affect the experimental yield (*vide infra*) and did not interfere with the yield calculation, which was always calculated on the basis of the original Klason lignin in the biomass. The reactor bed consisted of a catalyst, which was the desired metal supported on activated carbon well mixed with fused crushed SiO_2. The bed volume was fixed at a given volume (~3.0 mL) to ensure the same retention time for each experiment. Initially, an excess quantity of catalyst (500 mg) was used to maximize the cleavage of ether linkages in the lignin. Guided by previous work,[20,22] we preformed the continuous reaction at 180 °C under 60 bar of H_2. The weight hour space velocity (WHSV) was 0.6 h^{-1}. After 6 hours time-on-stream (TOS), the continuous hydrogenolysis using Ni/C as the catalyst (Fig. 2A, Table S1†) led to stable yields of monophenolic monomers corresponding to a yield of about 45% of the original Klason lignin, which was nearly identical to that of the batch reaction and close to the theoretical yield estimated by RCF of the biomass (50%). The major products were propylguaiacol (M1) and propylsyringol (M4) with higher than 99% selectivity. Dihydroconiferyl (M3) and dihydrosinapyl alcohol (M7) were barely detected, whereas they were produced in greater quantities (5–10% selectivity) in a batch reaction at similar conditions. The near complete selectivity toward pro-

pylphenols was likely explained by the *in situ* conversion of phenylpropanols due to the large excess of catalyst, following a reaction pathway that we have previously verified.[26]

We also used Ru/C as a catalyst for continuous hydrogenolysis at the same reaction conditions (Fig. 2C, Table S2†). At early TOS, some cyclohexane derivatives and ethylsyringol were generated and their content decreased as the operation progressed. The monomer yield reached about 40% at 20 h and remained stable for 80 h TOS. Propylphenols (M1, M4) and phenylpropanols (M3, M7) were the predominant products with a selectivity of 65% and 33%, respectively.

In both cases, the system was continuously run for 80–125 h and the yield and selectivity of monomers were stable, indicating no obvious catalyst deactivation occurred. The S/G ratio of the resulting monophenolic monomers was only slightly higher than that present in the native feedstock (about 80/20 as reported in our previous work[27]), which is not unexpected given that there can be more G units within C–C-linked monomers. The stable yield of monomers with TOS proved to be an artifact of having excess catalyst and running at full lignin conversion. We increased the WHSV to 2.4 h^{-1} by decreasing the amount of catalyst packed in the reactor to 125 mg. When using Ni/C as catalyst (Fig. 2B, Table S3†), the monomer yield reached 42% at 10 h as seen previously, but
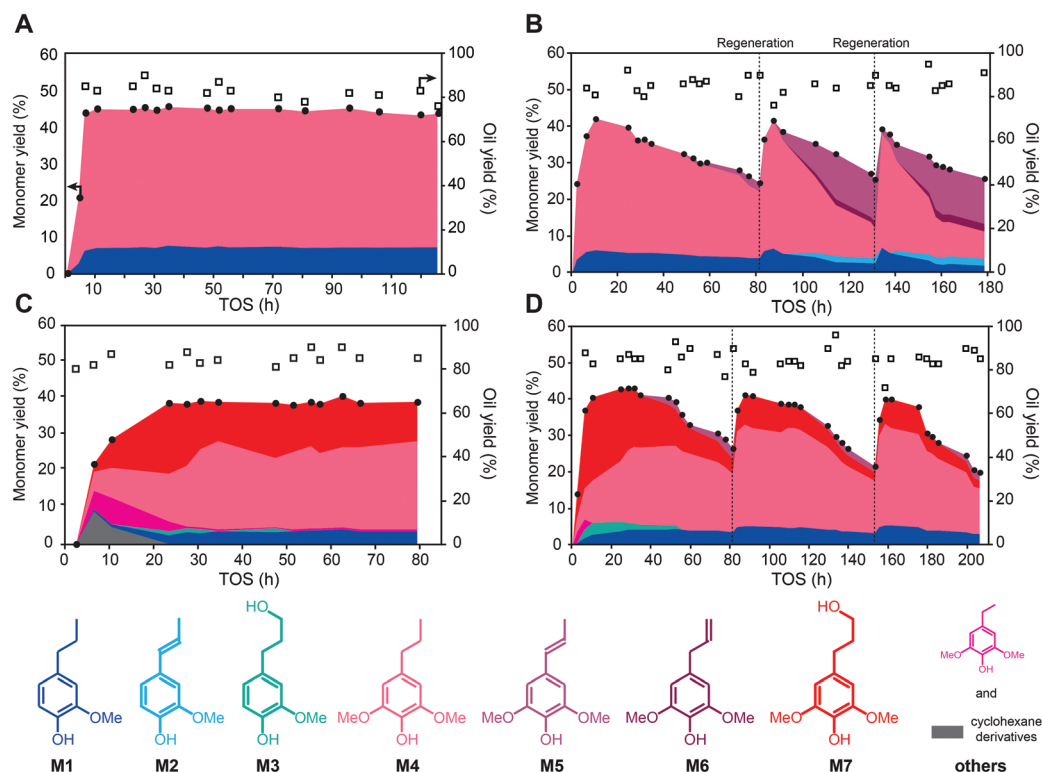

Fig. 2 Monophenolic monomer and oil yield produced from stabilized lignin depolymerized in a flow reactor A–D and their individual monomer structure. The feed solution consisted of 2.5 mg mL^{-1} stabilized lignin in dioxane/methanol (2 : 8, v/v), which was injected into the reactor at 0.1 mL min^{-1} by an HPLC pump. The oven was set at 180 °C. The H_2 pressure was set to 60 bar by a back pressure regulator and the flow rate of H_2 was 50 mL min^{-1}. The catalyst (A 500 mg of 5% Ni/C, B 125 mg of 5% Ni/C, C 500 mg of 5% Ru/C, D 125 mg of 5% Ru/C) was packed into a quarter inch tube with silicon dioxide (A and C 3000 mg, B and D 3500 mg). The dashed lines in B and D indicate the *in situ* reduction of the spent catalyst with H_2 at 450 °C for 5 h.

gradually declined to a yield of 25% at 80 h. At the same time, small quantities of unsaturated intermediates that were thought to be produced by solvolysis[20,29] (propenylsyringol, M5) were detected after 50 h. These results clearly indicated that the catalyst was deactivating as the reaction progressed. We tried to regenerate the catalyst *in situ* by flowing H_2 at 450 °C for 5 h in the absence of substrate flow. Calcination was deemed unsuitable for regeneration because of the activated carbon structure of the support. In the first few hours TOS after reduction, the monomer yield recovered to 42%. However, the yield decreased again to 26%, this time in a shorter period compared to the run with fresh catalyst. Moreover, the quantity of propenylphenols, including propenylsyringol (M5), iso-propenylsyringol (M6), and propenylguaiacol (M2), increased significantly during TOS, and ended up reaching a 60% selectivity at 130 h TOS. As the presumed hydrogenolysis mechanism of lignin includes both solvolysis and hydrogenation steps,[21,29] catalyst deactivation unsurprisingly appears to predominantly affect hydrogenation, which lead to an increased fraction of solvolysis intermediates. Moreover, the C=C bonds on the side chain make these products unstable as they can participate in condensation reactions, which likely contributed to the decrease in yield that we observed.[14] We repeated the regeneration process and observed a similar response in the yield and selectivity of monophenolic monomers (Fig. 2B).

A similar flow experiment using Ru/C led to similar deactivation patterns (Fig. 2D, Table S4†). *In situ* reduction of the catalyst allowed for a similar activity recovery and associated monomer yield. However, the regenerated bed again led to a faster deactivation and drop in monomer yield compared to the initial run. Interestingly, unlike the reactions run with Ni/C, we never observed substantial quantities of propenylphenols (M2, M5 and M6 always represented a selectivity of less

than 10%). The functions of the metal catalyst are mainly (1) accelerating of the β-O-4 cleavage and (2) hydrogenation of the C=C bonds to stabilize the lignin hydrogenolysis products. A previous study showed that the presence of a metal catalyst only slightly increased the rate of β-O-4 cleavage in batch reaction. However, we performed a control experiment without metal catalyst (only SiO_2 in the packed reactor) under the same condition as that showed in Fig. 2A, and only 4.5% of monophenolics (sinapyl alcohol and propenylsyringol M5) were detected by GC (Table S5†). HSQC characterization of the corresponding lignin oil showed that acetal stabilized lignin was maintained largely intact under these conditions (Fig. 3A), whereas the lignin oil recovered from the experiment shown on Fig. 2A showed full conversion of β-O-4 units and that substantial quantities of propylphenols were generated (Fig. 3B). This result indicated that the metal catalyst significantly accelerated the cleavage of acetal and β-O-4 under flow condition. Ni/C and Ru/C showed similar deactivation rates and generated similar monophenolics yields, whereas the selectivity towards side-chain unsaturated products was remarkably different. This difference as the reaction progressed suggested that Ni/C and Ru/C have a similar ether cleavage activity but Ru has a greater hydrogenation activity.[30,31]

We evaporated the solvent of each collected sample to measure the oil recovery (monomers, dimers, and oligomers) by weight. Oil yields remained around 80 to 90 wt% regardless of catalyst deactivation. Since each protected β-O-4 unit lost two oxygen atoms and a volatile propylidene acetal derivative to generate a propylphenol, and assuming a 60% β-O-4 linkage content in the lignin,[27] we can estimate that a mass loss of 27% and 30 wt%, would occur for each guaiacol and syringol unit, respectively. Furthermore, elemental analysis of the native lignin and whole mixture of hydrogenolysis products
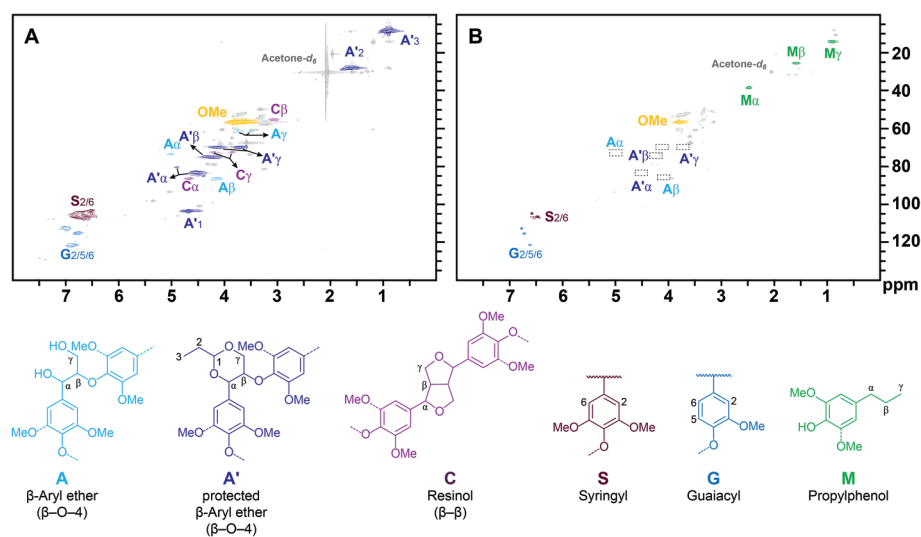

Fig. 3 HSQC spectra of lignin oil from continuous hydrogenolysis process and the corresponding structures. A: The catalyst bed consisted of only SiO_2 without any metal catalyst, corresponding to experiment in Table S5;† B: the catalyst bed consisted of 500 mg 5 wt% Ni/C mixed with SiO_2, corresponding to experiment in Fig. 2A and Table S1.†

resulting from the experiment depicted in Fig. 2B showed that the oxygen content decreased from 35% to 31% after hydrogenolysis, while the carbon content increased from 59% to 61% (see section 7 of the ESI†). Based on these two effects, we estimated that the yield of lignin oil should range between 81 and 88 wt% (see section 8 of the ESI†), which indicated that hydrogenolysis products were likely quantitatively recovered.

In order to better characterize catalytic lignin hydrogenolysis and the rate of catalyst deactivation under flow condition, we further estimated the turnover number (TON) and turnover frequency (TOF) in terms of monophenolic monomer yield, using the reaction over the Ni/C catalyst. TOF and TON were calculated by considering the active sites to be the accessible metal atoms measured by H_2 chemisorption. For the experiment in Fig. 2B, the TON was 24.7 before the catalyst deactivated, *i.e.*, the point at which the monophenolic monomer yield started to decrease (here we used the first 4 samples for calculation). On the other hand, the TON for the whole TOS in the experiment showed in Fig. 2A was 36.8. Even though it was substantially higher than the one calculated for the experiment in Fig. 2B, product analysis showed no signs of catalyst deactivation, suggesting that a higher catalyst loading (resulting in lower WHSV) reduced the catalyst deactivation rate. The estimated TONs of each run (assuming the regeneration process led to full recovery of the active sites) in the experiment showed in Fig. 2B decreased from 60.7 to 44.7 and 38.7 over similar TOS. Runs using Ru/C as the catalyst also showed similar trend (Fig. S3†). To evaluate the TOF of lignin hydrogenolysis over Ni/C, we further increased the WHSV to 8, 36, and 48 h^{-1} (Tables S6–S8†) to attempt to capture an extrapolated rate at zero conversion. Reaching higher WHSVs was complicated due to the limitation associated with producing large quantities of lignin at laboratory scale. Nevertheless, we were able to extrapolate a zero-conversion rate. In each experiment, the sample that reached the highest monophenolic yield was used to calculate the reaction rate, and the results were 3.55, 8.68, and 10.41 h^{-1}, respectively. These data were fit with a linear regression and extrapolated to zero yield, where a TOF of 15.97 h^{-1} was calcualted (Fig. S4†). A previous study showed that the TOF over Pd/C was 3.06–6.77 h^{-1} based on guaiacol production from a dimeric model compound between 105–120 °C.[24] The reported activation energies allowed us to calculate a turnover frequency of 125–253 h^{-1} for this system, which is one order of magnitude higher than our estimated TOF. This difference is likely due to the additional steric hinderance of the lignin polymer *vs.* a simple dimer that could significantly slow the reaction rate. In addition, rates obtained with Ni could be slightly lower than those achievable with Pd. We were able to use this rate, which is the highest available rate theoretically observed during the flow process, to verify the absence of mass transfer limitations. Using a criterion-based approach, we were able to verify that the characteristic diffusion time was around ~10^3 times higher than the characteristic reaction time, confirming that we are accurately measuring lignin hydrogenolysis kinetics (see section 9 in the ESI†).

Table 1 ICP measurement of the fresh and spent catalysts, and the collected liquor after reaction

	Ni	Ru
Fresh catalyst	5.20 wt%	5.10 wt%
Spent catalyst 1	5.23 wt%	5.00 wt%
Spent catalyst 2	5.31 wt%	5.06 wt%
Collected liquor 1[a]	0.10 wt%	0.07 wt%
Collected liquor 2[a]	0.05 wt%	0.02 wt%

[a] The metal content in the hydrogenolysis liquor was calculated as the detected amount of metal in the liquor over the total amount of metal in the original fresh catalyst.

After the reaction, we recovered and characterized the spent catalyst to better understand the underlying phenomena governing catalyst deactivation. ICP measurements of the spent catalysts recovered from the experiments shown on Fig. 2 all showed similar metal content as the fresh catalysts. The hydrogenolysis liquor collected from these experiments contained trace amount of Ni or Ru, corresponding to only 0.01–0.1 wt% of the total metal on the fresh catalyst (Table 1). Therefore, metal leaching did not seem to play an important role in catalyst deactivation. This result was markedly different than those reported for semi-continuous RCF systems with the same catalyst (Ni/C), where flowing the recently extracted liquor through a hydrogenation catalyst led to a decrease in metal content between 13.5 and 9.8 wt% after 12 h TOS. The authors demonstrated that biomass components were mainly responsible for leaching.[20] Organic acids, which notably includes the significant acetate fraction linked to hemicellulose, is likely to greatly enhance metal leaching due to the strong propensity of acetate to bind to metals such as Ni. In our approach, the hemicellulose is similarly solubilized during the initial fractionation step, but was largely separated from the lignin fraction during isolation. Given the highly detrimental effect of leaching on overall process operation and economics, limiting its occurrence by isolating the lignin could be an interesting feature of the AAF approach when considering various lignin valorization approaches. However, since deactivation still occurred (*vide infra*), challenges remain before any technology can be implemented industrially.

Transmission electron microscopy (TEM) was used to image and characterize the metal nanoparticle sizes of fresh and spent catalysts and determine their corresponding distributions (Fig. 4). The Ni nanoparticles clearly sintered forming several large particles with diameter >15 nm after about 180 h TOS. Some extremely large nickel particles (diameter >65 nm) were also spotted by TEM imaging and further verified by high-angle annular dark-field (HAADF) TEM, including using energy-dispersive X-ray spectroscopy to verify their composition (Fig. 4B and S5†). Ru/C also underwent particle growth but less substantially compared to Ni/C (Fig. 4D), which was indicative of the better thermal stability of Ru during lignin hydrogenolysis. This improved stability could also explain why we did not see the appearance of unsaturated products with Ru, where limited sintering let this metal maintaining
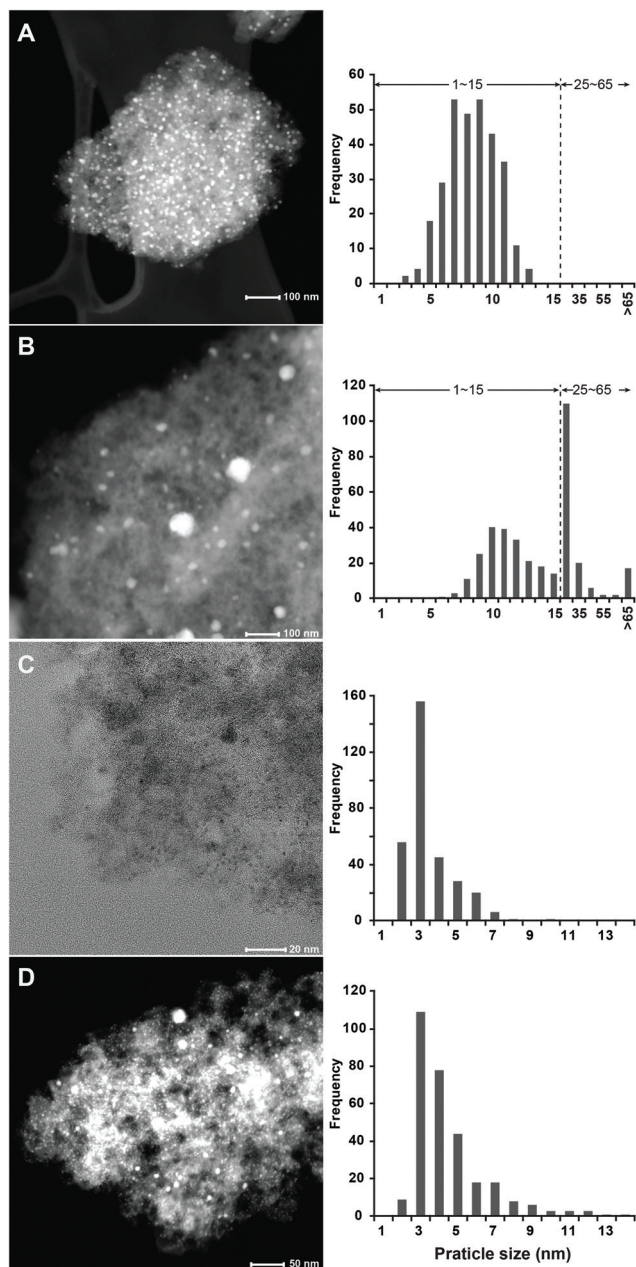
Fig. 4 TEM images of the fresh and spent catalysts (A–D) and the resulting particle size distributions. A: Fresh Ni/C; B: spent Ni/C resulting from the experiment shown in Fig. 2B; C: fresh Ru/C; D: spent Ru/C from the experiment shown in Fig. 2D. The histograms were calculated by analyzing the TEM images in panels A–D (from top to bottom), respectively.

Table 2 Physisorption and chemisorption characterization of the catalyst

	BET surface area[a] (m^2 g^{-1})	Pore volume[a] (cm^3 g^{-1})	Metal dispersion[b]
Fresh Ni/C	1022 ± 2	0.76	18%
Spent Ni/C	698 ± 3	0.64	14%
Spent Ni/C	312 ± 2	0.35	4%
Fresh Ru/C	729 ± 2	0.62	44%
Spent Ru/C	308 ± 1	0.39	40%
Spent Ru/C	216 ± 1	0.34	10%

[a] BET surface area and pore volume were determined by N$_2$ physisorption. [b] Metal dispersion was determined by the quantity of surface metal (determined by H$_2$ chemisorption) over the amount of total metal present.

sorption on both fresh and spent catalysts (Table 2). The BET surface area of spent Ni/C decreased compared to the fresh catalyst after 60 h TOS (from 1022 to 698 m^2 g^{-1}) and continued to do so after the subsequent 180 h TOS (reaching 312 m^2 g^{-1}). The total pore volume (Table 2 and Fig. S6†) was also reduced from 0.75 cm^3 g^{-1} to 0.64 and 0.35 cm^3 g^{-1} after hydrogenolysis of lignin for 60 and 180 h TOS, respectively. The BET surface area and pore volume of spent *vs.* fresh Ru/C showed a similar evolution. These results indicated that lignin residues had likely deposited and accumulated during hydrogenolysis in flow. The active sites on the catalyst were characterized by H$_2$ chemisorption and the associated metal dispersion was calculated (see section 6.2 in ESI† for calculations). The dispersion of spent Ni/C after 180 h TOS (corresponding to the experiment shown in Fig. 2B) decreased substantially from 18% to 4%, which was consistent with the TEM result and the simulation result of metal dispersion, showing significant sintering. In parallel, the dispersion of Ru/C measured by chemisorption declined from 44% to 10%, which was far greater than estimated by TEM (29 to 20%). However, TEM cannot distinguish between accessible and inaccessible metal nanoparticles, which could indicate that the loss of active sites on Ru/C was likely also due to irreversible carbonaceous deposits.

In order to evaluate the impact of regeneration process on the catalyst, we also performed an experiment using the same condition as those shown in Fig. 2B but stopped the reaction at around 80 h TOS (*i.e.* the point that the catalyst showed significant deactivation) and recovered the spent catalyst without regeneration. TEM images showed the presence of large nickel particles (>100 nm, Fig. S7A†) and H$_2$ chemisorption determined that Ni dispersion was only 6% (Fig. S7E†). These results were similar to the catalyst used for longer reaction times, which had been regenerated twice (Fig. 2B), indicating that the regeneration process likely did not contribute to metal nanoparticle sintering. On the other hand, the BET surface (Fig. S7D†) and total pore volume (Fig. S7B and C†) were 678 m^2 g^{-1} and 0.56 cm^3 g^{-1}, respectively, which was lower than the fresh catalyst, indicating the carbonaceous deposition on the catalyst surface had likely occured.

sufficient hydrogenation activity. Using these particle size distributions, we estimated the metal dispersion using a calculation based on an assumed metal nanoparticle geometry of truncated cubic octahedron model (see section S6.3 and Fig. S2†). This estimate led to a dramatic estimated decrease in dispersion for Ni/C from 14% to only 1% and a lesser decrease for Ru/C from 29% to 20%.

To further characterize the change in surface properties of the catalysts during deactivation, we also performed N$_2$ physi-

Metal oxides could in principle be promising supports for alleviating the issue of carbonaceous deposits because of the thermal stability of oxides during regeneration by calcination compared to carbon. In addition, several strategies have been developed to curtail sintering of metal nanoparticles supported on metal oxides.[32–36] For these reasons, we investigated the hydrogenolysis of lignin using several catalysts supported on metal oxides, including Ni/SiO_2, Ni/SiO_2-Al_2O_3, and Ni/TiO_2, but none of them was able to provide comparable monomer yields under flow conditions despite interesting results in batch (Table S11†). Control experiments in the batch reactor (Table S11†) were performed with only the support (without metal nanoparticles) and without any solid catalyst in MeOH, resulted in substantial quantities of monophenolic monomers (13–22%), whereas those in THF resulted in much lower yields (<7%), indicating that all the solvent, support, and metal nanoparticles play important roles during lignin hydrogenolysis. We also characterized the metal oxide catalysts by physisorption and TEM (Table S12†), but the results did not indicate a clear correlation between monomer yields and BET surface, pore volume, or metal dispersion. Further study is required to understand why carbon supports perform better than metal oxide supports during batch and continuous AAF lignin hydrogenolysis.

3. Conclusion

In this study we demonstrated that lignin could be upgraded in flow in a fully continuous and steady state manner. Using propylidene acetal stabilized lignin extracted from birch, we were able to show that monophenolic monomers could be produced at high yields (up to 45% over Ni/C and 40% over Ru/C based on Klason lignin content), which were comparable to batch operation. However, when using catalyst loadings that were not in excess of those required to reach maximum yields, we observed rapid catalyst deactivation that was due to metal sintering and blocking of active sites due to presumed lignin deposition. The successful demonstration of high yield lignin upgrading in a truly continuous and steady state operation allows us to more clearly analyze these deactivation mechanisms as well as accurately estimate lignin hydrogenolysis rates. Further efforts are needed to suppress sintering and minimize the effect of carbonaceaous deposition to enable long term continuous operation and allow lignin depolymerization to become affordable. Nevertheless, our study provides a useful tool to better understand the limitations and opportunities of continuous lignin valorization as well as a platform for studying, designing and testing heterogeneous catalysts for lignin hydrogenolysis.

4. Experimental section

Detailed experimental procedures for the lignin extraction, catalyst characterization, and monomers quantitation are avail-

able in the ESI.† The continuous lignin hydrogenolysis was performed on a custom-built flow reactor system. A quarter inch tube (~42 cm in length) packed with catalyst and fused crushed silicon dioxide (see Fig. S1†) was used as reactor and placed in a vertical split furnace. The reaction temperature was then set to 180 °C. The feedstock that was used consisted of the protected lignin in a dioxane/methanol solution (2 : 8, v/v) at a concentration of 2.5 mg mL^{-1} or 5.0 mg mL^{-1}. The solution was filtered to eliminate any potential precipitate before the reaction to avoid clogging issue during the process. The feed rate was set at 0.1–0.4 mL min^{-1}. The flow rate of H_2 was set at 50 mL min^{-1} and the pressure was set at 60 bar. The hydrogenolysis liquor was collected and analyzed by GC-MS and GC-FID. After the reaction, the catalyst was recovered along with the SiO_2 for TEM, physisorption, and chemisorption study.

Author contributions

W.L. and J.L. designed the project. J.L. supervised the project. W.L. performed all the experiments unless mentioned otherwise. Y.P. performed the TEM characterization. S.S. and J.B. performed part of the studies with of the metal oxide supports. F.H. provided technical assistance to W.L. on the physisorption and chemisorption study and data analysis. W.L. and J.L. wrote the manuscript and all authors edited the article.

Conflicts of interest

The authors declare the following competing financial interest (s): F. H., J. B. B. and J. S. L. are part owners in Bloom Biorenewables Ltd, which is exploring commercial opportunities for stabilized lignin.

References

1 W. Boerjan, J. Ralph and M. Baucher, *Annu. Rev. Plant Biol.*, 2003, **54**, 519–546.

2 R. Rinaldi, R. Jastrzebski, M. T. Clough, J. Ralph, M. Kennema, P. C. A. Bruijnincx and B. M. Weckhuysen, *Angew. Chem., Int. Ed.*, 2016, **55**, 8164–8215.

3 W. Schutyser, T. Renders, S. Van den Bosch, S. F. Koelewijn, G. T. Beckham and B. F. Sels, *Chem. Soc. Rev.*, 2018, **47**, 852–908.

4 P. Sudarsanam, R. Y. Zhong, S. Van den Bosch, S. M. Coman, V. I. Parvulescu and B. F. Sels, *Chem. Soc. Rev.*, 2018, **47**, 8349–8402.

5 Z. H. Sun, B. Fridrich, A. de Santi, S. Elangovan and K. Barta, *Chem. Rev.*, 2018, **118**, 614–678.

6 S. Van den Bosch, S. F. Koelewijn, T. Renders, G. Van den Bossche, T. Vangeel, W. Schutyser and B. F. Sels, *Top. Curr. Chem.*, 2018, **376**(36), DOI: 10.1007/s41061-018-0214-3.

7 T. Renders, G. Van den Bossche, T. Vangeel, K. Van Aelst and B. Sels, *Curr. Opin. Biotechnol.*, 2019, **56**, 193–201.

8 S. B. Baker and H. Hibbert, *J. Am. Chem. Soc.*, 1948, **70**, 63–67.

9 C. P. Brewer, L. M. Cooke and H. Hibbert, *J. Am. Chem. Soc.*, 1948, **70**, 57–59.

10 J. M. Pepper and H. Hibbert, *J. Am. Chem. Soc.*, 1948, **70**, 67–71.

11 Y. D. Li, S. D. Karlen, B. Demir, H. Kim, J. Luterbacher, J. A. Dumesic, S. S. Stahl and J. Ralph, *ChemSusChem*, 2020, **13**(17), 4487–4494.

12 Y. M. Questell-Santiago, M. V. Galkin, K. Barta and J. S. Luterbacher, *Nat. Rev. Chem.*, 2020, **4**, 311–330.

13 T. Phongpreecha, N. C. Hool, R. J. Stoklosa, A. S. Klett, C. E. Foster, A. Bhalla, D. Holmes, M. C. Thies and D. B. Hodge, *Green Chem.*, 2017, **19**, 5131–5143.

14 W. Lan and J. S. Luterbacher, *Chimia*, 2019, **73**, 591–598.

15 N. Yan, C. Zhao, P. J. Dyson, C. Wang, L. T. Liu and Y. Kou, *ChemSusChem*, 2008, **1**, 626–629.

16 J. S. Luterbacher, A. Azarpira, A. H. Motagamwala, F. Lu, J. Ralph and J. A. Dumesic, *Energy Environ. Sci.*, 2015, **8**, 2657–2663.

17 Q. Song, F. Wang, J. Y. Cai, Y. H. Wang, J. J. Zhang, W. Q. Yu and J. Xu, *Energy Environ. Sci.*, 2013, **6**, 994–1007.

18 S. Van den Bosch, W. Schutyser, S. F. Koelewijn, T. Renders, C. M. Courtin and B. F. Sels, *Chem. Commun.*, 2015, **51**, 13158–13161.

19 S. Van den Bosch, W. Schutyser, R. Vanholme, T. Driessen, S. F. Koelewijn, T. Renders, B. De Meester, W. J. J. Huijgen, W. Dehaen, C. M. Courtin, B. Lagrain, W. Boerjan and B. F. Sels, *Energy Environ. Sci.*, 2015, **8**, 1748–1763.

20 E. M. Anderson, M. L. Stone, R. Katahira, M. Reed, G. T. Beckham and Y. Román-Leshkov, *Joule*, 2017, **1**, 613–622.

21 E. M. Anderson, M. L. Stone, M. J. Hulsey, G. T. Beckham and Y. Román-Leshkov, *ACS Sustainable Chem. Eng.*, 2018, **6**, 7951–7959.

22 I. Kumaniaev, E. Subbotina, J. Savmarker, M. Larhed, M. V. Galkin and J. S. M. Samec, *Green Chem.*, 2017, **19**, 5767–5771.

23 V. Molinari, G. Clavel, M. Graglia, M. Antonietti and D. Esposito, *ACS Catal.*, 2016, **6**, 1663–1670.

24 Y. D. Li, B. Demir, L. M. V. Ramos, M. J. Chen, J. A. Dumesice and O. Ralph, *Green Chem.*, 2019, **21**, 3561–3572.

25 L. Shuai, M. T. Amiri, Y. M. Questell-Santiago, F. Heroguel, Y. D. Li, H. Kim, R. Meilan, C. Chapple, J. Ralph and J. S. Luterbacher, *Science*, 2016, **354**, 329–333.

26 W. Lan, M. T. Amiri, C. M. Hunston and J. S. Luterbacher, *Angew. Chem., Int. Ed.*, 2018, **57**, 1356–1360.

27 W. Lan, J. B. de Bueren and J. S. Luterbacher, *Angew. Chem., Int. Ed.*, 2019, **58**, 2649–2654.

28 M. T. Amiri, G. R. Dick, Y. M. Questell-Santiago and J. S. Luterbacher, *Nat. Protoc.*, 2019, **14**, 921–954.

29 S. Van den Bosch, T. Renders, S. Kennis, S. F. Koelewijn, G. Van den Bossche, T. Vangeel, A. Deneyer, D. Depuydt, C. M. Courtin, J. M. Thevelein, W. Schutyser and B. F. Sels, *Green Chem.*, 2017, **19**, 3313–3326.

30 C. Michel and P. Gallezot, *ACS Catal.*, 2015, **5**, 4130–4132.

31 J. C. Lee, Y. Xu and G. W. Huber, *Appl. Catal., B*, 2013, **140**, 98–107.

32 Y. P. Du and J. S. Luterbacher, *Chimia*, 2019, **73**, 698–706.

33 H. B. Zhang, Y. Lei, A. J. Kropf, G. H. Zhang, J. W. Elam, J. T. Miller, F. Sollberger, F. Ribeiro, M. C. Akatay, E. A. Stach, J. A. Dumesic and C. L. Marshall, *J. Catal.*, 2014, **317**, 284–292.

34 Y. P. Du, F. Heroguel and J. S. Luterbacher, *Small*, 2018, **14**, 1801733.

35 Y. P. Du, F. Héroguel, X. T. Nguyen and J. S. Luterbacher, *J. Mater. Chem. A*, 2019, 23803–23811, DOI: 10.1039/C9TA01459D.

36 F. Heroguel, B. P. Le Monnier, K. S. Brown, J. C. Siu and J. S. Luterbacher, *Appl. Catal., B*, 2017, **218**, 643–649.